Ion Transfer across Liquid–Liquid Phase Boundaries: Electrochemical Kinetics by Faradaic Impedance

Thomas Wandlowski,† Vladimir Mareček, Karel Holub, and Zdeněk Samec*

J. Heyrovský Institute of Physical Chemistry and Electrochemistry, Czechoslovak Academy of Sciences, Dolejškova 3, 182 23 Prague 8, Czechoslovakia *(Received: September 6, 1988; In Final Form: April 27, 1989)*

Ion transport rates across the water–nitrobenzene interface have been determined by faradaic impedance measurements at equilibrium potentials. Lithium chloride and tetrabutylammonium tetraphenylborate (or tetraphenylarsonium dicarbollylcobaltate) were used as supporting electrolytes. First-order ion-transfer kinetics across the phase boundary were substantiated for bulky anions and cations. The potential dependence of the relevant heterogeneous rate constants was similar to the classical Butler–Volmer equation for conventional electrochemical rate constants. This finding is accounted for by a three-step mechanism. Ion transfer across a rigid layer of solvent molecules at the phase boundary was the rate-determining step. That compact layer was "sandwiched" between two space charge layers and presented a potential barrier of 14–17 kJ mol^{-1}. Based on these results, limiting rates were estimated for the solvent extraction of picrates and perchlorates from water into nitrobenzene.

Introduction

Liquid–liquid interfacial kinetics has attracted much attention in the recent past.[1] Work has been focused on the simple transfer of soluble solutes from the aqueous to the organic (oil) phase or vice versa

$$\text{solute (w)} \rightleftarrows \text{solute (o)} \qquad (1)$$

eventually assisted by an oil-soluble complexing agent.[1,2] Theoretical models and methods for kinetic measurements were reviewed and their applicability discussed.[2] One of the more sophisticated approaches to the study of the interfacial kinetics has been through direct measurements of the ion-transfer rates across the interface between two immiscible electrolyte solutions (ITIES) by various electrochemical techniques.[3] We have been interested in using cyclic[4] or convolution potential sweep[5] voltammetry for this purpose. Others have employed galvanostatic pulse,[6] phase-selective ac polarographic[7] or faradaic impedance[8] techniques. However, the evaluation of ion-transfer rates from measurements involving large potential sweeps and variations can be uncertain. This is mainly because of the considerable ohmic potential drop, which must be compensated or subtracted in potentiostatic or galvanostatic experiments. Moreover, mechanical instabilities of the ITIES arising from the potential dependence of the surface tension[9] can influence the ion transport. For these reasons, the application of a small signal exciting the system in the thermodynamic equilibrium should offer more reliable kinetic data.[10] Unfortunately, data obtained in this way are few and inconsistent. Impedance measurements of the equilibrium pictrate ion transfer across the water–nitrobenzene interface[10] indicated that ionic rate constants can be as high as about 0.1 cm s^{-1}. Consequently, those evaluated from direct current measurements[5-7] are underestimated by a factor 2 or 3. On the other hand, ionic rate constants as low as about 5×10^{-3} cm s^{-1} have been reported for some tetraalkylammonium ions and perchlorate.[8]

In the present paper we aim at a better understanding of the mechanism of the ion transport across the ITIES. For this purpose, the transfer of series of monovalent (tetraalkylammonium, tetraalkylphosphonium) and divalent (dialkyldipyridinium) cations and of perchlorate anion was studied by an equilibrium impedance technique. As compared with literature data, the present results definitely point to a faster (and in some cases distinctly faster) ion transport kinetics. These results are of consequence for the analysis of the molecular mechanism of the ion transport as well as for the prediction of extraction rates for corresponding salts.

Experimental Section

Materials. LiCl (purum, p.a., Fluka) and tetrabutylammonium tetraphenylborate (Bu_4NPh_4B) or tetraphenylarsonium 3,3-*commo*-bis(undecahydro-1,2-dicarba-3-cobalta-*closo*-dodecaborate) (Ph_4AsDCC) were used for preparation of base-electrolyte solutions in double-distilled water and nitrobenzene (puriss., p.a., Fluka). Tetraalkylammonium and trimethylalkylphosphonium tetraphenylborates (R_4NPh_4B, Me_3RPPh_4B) and *N,N'*-dialkyl-4,4'-dipyridinium bis(tetraphenylborate)s ($R_2V(Ph_4B)_2$), with R = methyl (Me), ethyl (Et), propyl (Pr), or butyl (Bu), were precipitated from corresponding quaternary ammonium or phosphonium hallogenides and sodium tetraphenylborate (Fluka). The product of this precipitation was recrystallized twice from acetone or water–acetone mixture. Ph_4AsDCC and *N,N'*-dialkyl-4,4'-dipyridinium dibromides were prepared as described in ref 11 and 12, respectively. $LiClO_4$, tetrabutylammonium perchlorate, tetraphenylarsonium chloride, and tetraalkylammonium chlorides and bromides, all purchased from Fluka as Reagent Grade chemicals, were used as received. The generous gift of trimethylalkylphosphonium bromides and iodides from Dr. M. Heinze, VEB Fahlberg-List Magdeburg (G.D.R.), is greatly acknowledged.

Apparatus. A block scheme of the apparatus is shown in Figure 1. A flat water–nitrobenzene interface with a geometric area of 19.2 mm^2 was formed in a four-electrode cell, which was described in detail elsewhere.[13] The cell was immersed in a water

† On leave from Päd. Hochschule "N.K. Krupskaja", Kröllwitzer Str. 44, Halle 4050, G.D.R.

(1) Mears, P. *Faraday Discuss. Chem. Soc.* **1984**, *77*, 7.
(2) Hanna, G. J.; Noble, R. D. *Chem. Rev.* **1985**, *85*, 583.
(3) Koryta, J. In *The Interface Structure and Electrochemical Processes at the Boundary Between Two Immiscible Liquids*; Kazarinov, V. E., Ed.; Springer Verlag: Berlin, 1987; p 3.
(4) (a) Samec, Z.; Mareček, V.; Weber, J. *J. Electroanal. Chem. Interfacial Electrochem.* **1979**, *100*, 841. (b) Samec, Z.; Mareček, V.; Koryta, J.; Khalil, M. W. *J. Electroanal. Chem. Interfacial Electrochem.* **1977**, *83*, 393. (c) Hanzlik, J.; Samec, Z. *Collect. Czech. Chem. Commun.* **1987**, *52*, 830.
(5) (a) Samec, Z.; Mareček, V.; Weber, J.; Homolka, D. *J. Electroanal. Chem. Interfacial Electrochem.* **1981**, *126*, 105. (b) Samec, Z.; Mareček, V. *J. Electroanal. Chem. Interfacial Electrochem.* **1986**, *200*, 17. (c) Samec, Z.; Mareček, V.; Homolka, D. *J. Electroanal. Chem. Interfacial Electrochem.* **1983**, *158*, 25.
(6) (a) Gavach, C.; d'Epenoux, B.; Henry, F. *J. Electroanal. Chem. Interfacial Electrochem.* **1975**, *64*, 107. (b) Melroy, O. R.; Buck, R. P. *J. Electroanal. Chem. Interfacial Electrochem.* **1982**, *136*, 19.
(7) (a) Osakai, T.; Kakutani, T.; Senda, M. *Bull. Chem. Soc. Jpn.* **1984**, *57*, 370. (b) Osakai, T.; Kakutani, T.; Senda, M. *Bull. Chem. Soc. Jpn.* **1985**, *58*, 2626.
(8) Buck, R. P.; Bronner, W. E. *J. Electroanal. Chem. Interfacial Electrochem.* **1986**, *197*, 179.
(9) Kakiuchi, T.; Senda, M. *Bull. Chem. Soc. Jpn.* **1983**, *56*, 1753.
(10) Wandlowski, T.; Mareček, V.; Samec, Z. *J. Electroanal. Chem. Interfacial Electrochem.* **1988**, *242*, 291.
(11) Janoušek, Z.; Plešek, J.; Heřmánek, S.; Baše, K.; Todd, L. J.; Wright, W. F. *Collect. Czech. Chem. Commun.* **1981**, *46*, 2818.
(12) Evans, A. G.; Evans, J. C.; Baker, M. W. *J. Chem. Soc., Perkin Trans.* **1977**, *2*, 1787.
(13) Mareček, V.; Samec, Z. *J. Electroanal. Chem. Interfacial Electrochem.* **1985**, *185*, 263.

0022-3654/89/2093-8204$01.50/0

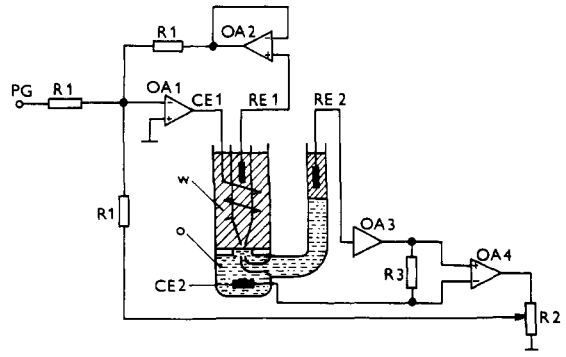

Figure 1. Scheme of the four-electrode potentiostatic assembly for the electrochemical polarization of an ITIES: CE1 and CE2 are counter electrodes, RE1 and RE2 are reference electrodes, PG is the pulse generator, OA is the operational amplifier, R is the resistor, and w or o denotes the aqueous or the organic solvent phase.

bath, the temperature of which was maintained at 293.0 ± 0.1 K. The potential difference $E = \varphi^{Ag} - \varphi^{Ag'}$ of the galvanic cell

Ag	AgCl	0.05 M LiCl + xMX^z (w)	0.05 M Bu_4NPh_4B or Ph_4AsDCC + yMX^z (o)	0.05 M Bu_4NCl or Ph_4AsCl (w′)	AgCl	Ag′

$$x, y = (0.1\text{–}1.0) \times 10^{-3}$$

where X^z represents the investigated ion, was controlled by means of a four-electrode potentiostat.[4a,14] The conversion of the potential E into the Galvani potential difference $\Delta_o^w\varphi = \varphi^w - \varphi^o$ was accomplished on the basis of the standard Galvani potential difference $\Delta_o^w\varphi^\circ_R = -0.275$ V[14] or −0.372 V[15] for the Bu_4N^+ or Ph_4As^+ ion transfer, respectively according to

$$E = \Delta_o^w\varphi + \Delta_w^{Ag}\varphi - \Delta_o^{Ag'}\varphi$$
$$= \Delta_o^w\varphi - \Delta_o^w\varphi^\circ_R + \Delta E' \qquad (2)$$

where R = Bu_4N^+ or Ph_4As^+. The activity coefficient term $\Delta E'$ = 7 mV was estimated from the extended Debye–Hückel theory.

Methods. Both cyclic voltammetry and impedance measurements were performed using a Solartron 1250 frequency response analyser (Solartron Instruments, England) operated by a 40 kbyte microcomputer. In the impedance measurements a small-amplitude (5 or 10 mV peak to peak) sinusoidal voltage (0.4–1000 Hz) was applied across the interface at the equilibrium potential, without using any ohmic potential drop compensation. The positive feedback (cf. Figure 1) was introduced only in the voltammetric measurements to compensate the solution resistance between 1.2 and 1.3 kΩ. The equilibrium potential was measured with a high-impedance voltmeter.

The analysis of complex impedances $\tilde{Z}_0$ and $\tilde{Z}_1$ of the water–nitrobenzene interface measured in the absence and presence of the ion X^z, respectively, was based on the following assmptions. First, the interface was represented by an electrical equivalent circuit, which consisted of the parallel combination of the interfacial capacitance $\tilde{Z}_c$, the faradaic impedance $\tilde{Z}_{f0}$ due to the transfer of base electrolyte ions, and the faradaic impedance $\tilde{Z}_{f1}$ due to the X^z ion transfer, with the solution resistance R_s in series. Second, the presence of the X^z ion was assumed to effect neither the structure of the electrical double layer nor the transfer of base electrolytes; i.e., their contribution were additive. Third, the impedance $\tilde{Z}_0$ was analyzed assuming that kinetic effects in the transfer of base electrolyte ions can be neglected.

The capacitance $\tilde{Z}_c$ was evaluated from measurements performed in the absence of the ion X^z by[16]

$$\tilde{Z}_c = (j\omega C_d)^{-1} = -jZ_0''[(X+1)^2 + 1]/X(X+1) \qquad (3)$$

TABLE I: Thermodynamic, Transport, and Kinetic Data for Transfer of Mono- and Divalent Ions across Water–Nitrobenzene Interface at 293 K[a]

ion	$\Delta_o^w\varphi^\circ$, mV	10^6D^w, $cm^2\ s^{-1}$	10^6D^o, $cm^2\ s^{-1}$	$10^2k_{app}^0$, $cm\ s^{-1}$	α_{app}
Me_4N^+	27	9.5	3.7	13.6	0.58
Et_4N^+	−67	9.3	4.0	9.0	0.64
Pr_4N^+	−170	8.5	3.4	13.6	0.60
Me_4P^+	9	8.8	3.7	14.8	0.55
Me_3EtP^+	−20	8.1	3.6	12.6	0.51
Me_3PrP^+	−50	6.7	3.1	12.6	0.58
Me_3BuP^+	−84	5.8	2.9	8.9	0.57
Pi^{-b}	39	6.1	2.7	8.3	0.56
ClO_4^-	−83	15.3	6.7	9.0	0.57
Me_2V^{2+}	−15	5.6	2.3	4.8	0.50
Et_2V^{2+}	−43	4.1	1.5	5.3	0.49
Pr_2V^{2+}	−58	3.3	0.9	6.8	0.55

[a] Base electrolytes: 0.05 M LiCl in water, 0.05 M Bu_4NPh_4B (or 0.05 M Ph_4AsDCC for Pr_4N^+ ion transfer) in nitrobenzene. [b] Data taken from ref 10.

where $j = (-1)^{1/2}$, ω is the angular frequency, C_d is the differential capacitance of the double layer, $X = Z_0''(Z_0' - R_s)^{-1}$ and Z_0' or Z_0'' are the real and the imaginary parts of the measured impedance $\tilde{Z}_0$. The solution resistance R_s was found as the high-frequency limit of $\tilde{Z}_0$. The faradaic impedance $\tilde{Z}_{f1}$ was calculated from the admittance $\tilde{Y}_{f1}$ corresponding to the X^z ion transfer[7a]

$$\tilde{Y}_{f1} = \tilde{Y}_1 - \tilde{Y}_0 \qquad (4)$$

where $\tilde{Y}_1$ and $\tilde{Y}_0$ are admittances corrected for the solution resistance R_s

$$Y_i' = \frac{(Z_i' - R_s)}{(Z_i' - R_s)^2 + Z_i''^2} \qquad i = 0, 1 \qquad (5)$$

$$Y_i'' = \frac{Z_i''}{(Z_i' - R_s)^2 + Z_i''^2} \qquad i = 0, 1 \qquad (6)$$

Results

Potentiometry. In the case when the bulk concentrations $c^{0,w}$ and $c^{0,o}$ of the ion X^z in the aqueous and organic phase differ from zero, the Nernst potential E

$$E = E^\circ + (RT/zF)\ln(c^{0,o}/c^{0,w}) + \Delta E'' \qquad (7)$$

should be established in the galvanic cell, which would correspond to the equilibrium in the ion-transfer reaction. Here E° is the standard potential difference $\Delta_o^w\varphi^\circ$ for the transfer of the ion X^z referred to that for the reference ion R; i.e., $E^\circ = \Delta_o^w\varphi^\circ - \Delta_o^w\varphi^\circ_R$ (cf. eq 2). The activity coefficient term $\Delta E''$ now includes contributions from the activity coefficients of the transferred ion X^z in water and nitrobenzene, which in the case of monovalent cations compensate for $\Delta E'$, i.e., $\Delta E'' \approx 2$ mV, whereas for divalent cations $\Delta E'' \approx -10$ mV and for monovalent anions $\Delta E'' \approx 12$ mV, as estimated from the extended Debye–Hückel equation.

Potentiometric measurements were carried out under conditions that (a) the total ion concentration $(x + y)$ or (b) the ion concentration in one phase only (x or y) were held constant and equal to 10^{-3} mol dm^{-3}. The concentration ratio (y/x) was varied by changing ion concentrations x and/or y in the range 10^{-4}–10^{-3} mol dm^{-3}. Figure 2 shows plots of the equilibrium potential difference $\Delta_o^w\varphi$ as a function of $\ln(c^{0,o}/c^{0,w})$. The linear regression analysis of these plots yields the slopes in the range from 24.5 to 25.5, −23.0 to −25.0, or 13.2 to 13.4 mV/decade for monovalent cations, monovalent anions, or divalent cations, respectively, with the correlation coefficient in the range 0.98–0.99. Values of standard potential differences $\Delta_o^w\varphi^\circ$ evaluated for monovalent ions from these plots are summarized in Table I.

The evaluation of standard potential differences for divalent cations is a more complicated task. In contrast to monovalent

(14) Samec, Z.; Mareček, V.; Homolka, D. *Faraday Discuss. Chem. Soc.* **1984**, *77*, 197.
(15) Koryta, J.; Vaňýsek, P.; Březina, M. *J. Electroanal. Chem. Interfacial Electrochem.* **1977**, *75*, 211.
(16) Mareček, V.; Samec, Z. *J. Electroanal. Chem. Interfacial Electrochem.* **1983**, *149*, 185.

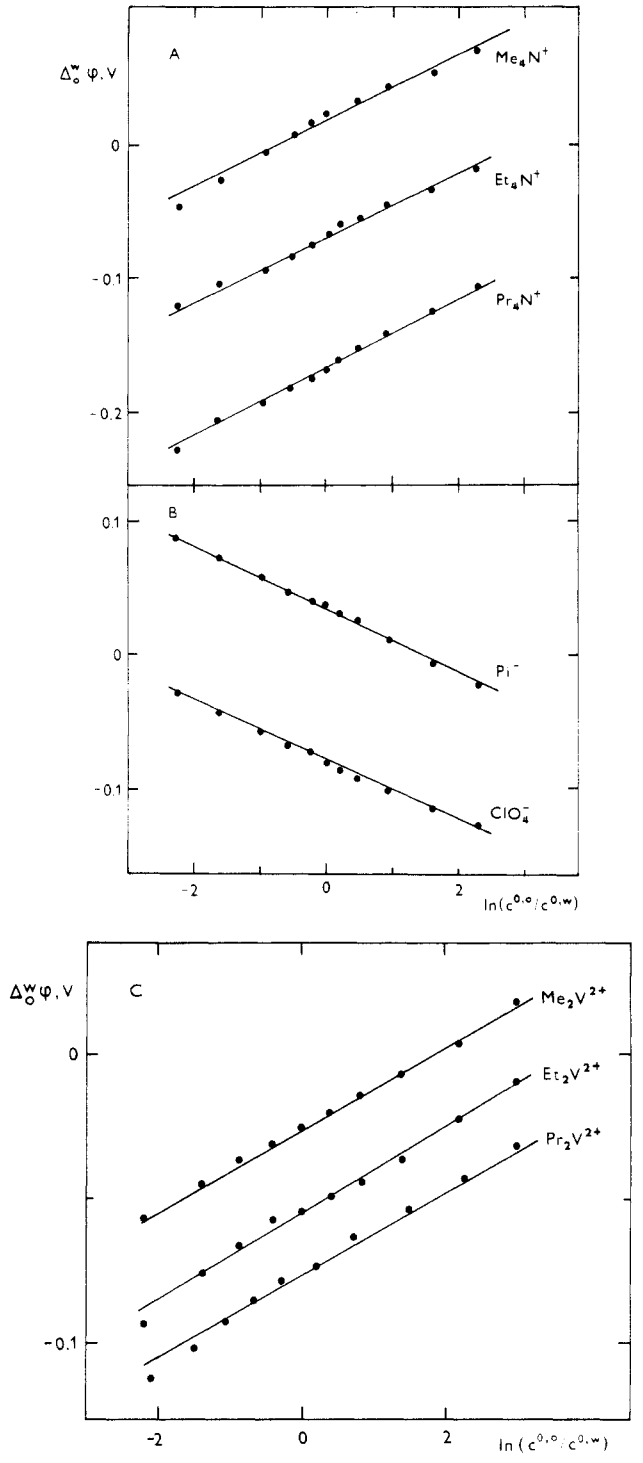

Figure 2. Equilibrium potential difference $\Delta_o^w\varphi$ vs ln $(c^{0,o}/c^{0,w})$ for the interface between 0.05 M LiCl in water and 0.05 M Bu_4NPh_4B or Ph_4AsDCC in nitrobenzene in the presence of (A) monovalent cations, (B) monovalent anions, and (C) divalent cations.

ions studied, R_2V^{2+} cations form ion pairs with Ph_4B^- in nitrobenzene.[4c] Instead of the simple ion transfer, facilitated ion transfer takes place; e.g., in the case of the 1:1 association[4c]

$$R_2V^{2+}(w) + Ph_4B^-(o) \rightleftarrows R_2VPh_4B^+(o) \qquad (8)$$

The standard potential $E^{o\prime} = \Delta_o^w\varphi^o - \Delta_o^w\varphi^o{}_R$ or the standard potential difference $\Delta_o^w\varphi^o$ for the simple transfer of R_2V^{2+} ion was evaluated from the equation

$$E^o = E^{o\prime} - (RT/2F) \ln [1 + K^o\gamma^o c^{0,o}] + \Delta E'' \qquad (9)$$

where E^o is the equilibrium value of the potential E at $c^{0,o}/c^{0,w} = 1$; cf. eq 7. The bulk concentration of the counterion Ph_4B^-

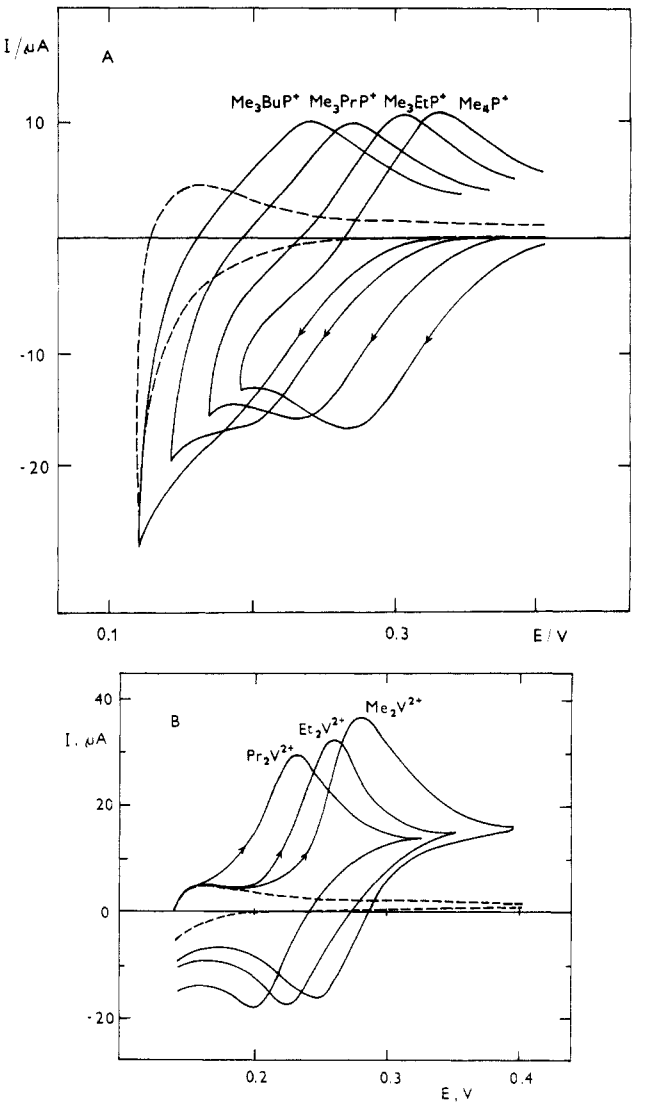

Figure 3. Voltammetric behavior of (A) monovalent cations ($c^{0,o} = 6 \times 10^{-4}$ mol dm^{-3}) and (B) divalent cations ($c^{0,w} = 4 \times 10^{-4}$ mol dm^{-3}) at the water–nitrobenzene interface at the scan rate of 50 mV s^{-1}. Dashed line: voltammogram of base electrolytes for each case.

$c^{0,o} = 0.05$ mol dm^{-3}, the activity coefficient of the R_2V^{2+} ion in nitrobenzene $\gamma^o = 0.12$ was estimated from the extended Debye–Hückel equation, and the association constants in nitrobenzene $K^o = 580$, 648, or 677 dm^3 mol^{-1} for Me_2V^{2+}, Et_2V^{2+}, or Pr_2V^{2+}, respectively, were taken from the literature.[4c] Results of these evaluations are also in Table I.

Cyclic Voltammetry. Figure 3 illustrates the voltammetric behavior of mono- and divalent cations observed for sweep rates of $v = 5$–100 mV s^{-1}. Regardless of whether the ion X^z was present in the aqueous ($x \neq 0$, $y = 0$) or nitrobenzene ($x = 0$, $y \neq 0$) phase, the peak current on the forward scan was proportional to both the square root of v and the ion concentration, while the peak potential difference was constant and equal to 58 ± 2 mV or 29 ± 2 mV for mono- and divalent cations, respectively. Diffusion coefficients D^w and D^o of ions in water and nitrobenzene and reversible half-wave potentials $E_{1/2}{}^{rev}$ were evaluated from voltammetric data by using the Nicholson–Shain theory.[17] $E_{1/2}{}^{rev}$ was used to evaluate the standard potential E^o or the standard potential difference $\Delta_o^w\varphi^o$, which agreed with potentiometric data, the difference being generally less than ±8 mV.

Impedance Measurements. Typical impedance plots are displayed in Figure 4. Impedance plots for base electrolytes were smooth curves, which did not exhibit any faradaic or even kinetic control in the frequency range 0.4–1000 Hz. On the other hand,

(17) Nicholson, R. S.; Shain, I. *Anal. Chem.* **1964**, *36*, 706.

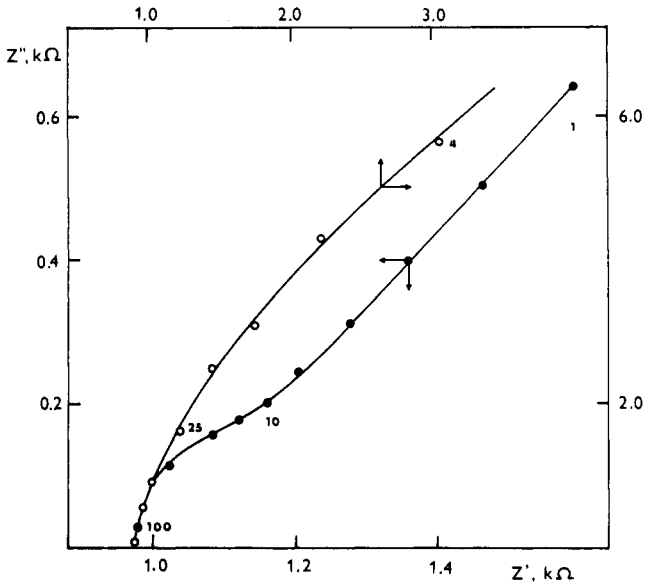

Figure 4. Impedance plots for the interface between 0.05 M LiCl in water and 0.05 M Bu_4NPh_4B in nitrobenzene in the absence (○) or in the presence (●) of Me_3PrP^+ ion ($c^{0,w} = c^{0,o} = 5 \times 10^{-4}$ mol dm^{-3}). Numbers on curves are frequencies in hertz.

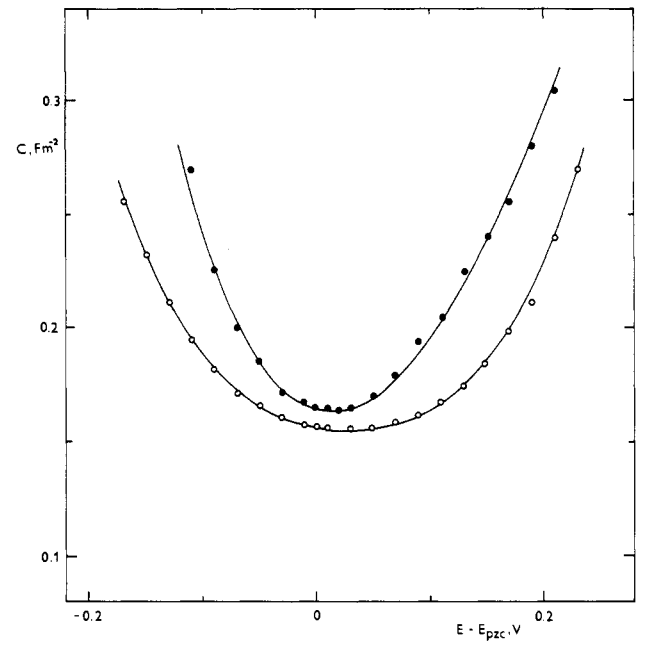

Figure 5. Differential capacitance of the double layer vs the potential at the interface between 0.05 M LiCl in water and 0.05 M Bu_4NPh_4B (●) or Ph_4AsDCC (○) in nitrobenzene.

the frequency region where the mass transport dominates was well-defined for the ion X^z, cf. the unity-slope plot at frequencies lower than about 25 Hz. Above 25 Hz the system showed a frequency-limited kinetic region. At the highest frequencies all impedance plots merged and reached the high-frequency limit, which was determined by the solution resistance R_s ($Z' = R_s$, $Z'' = 0$).

The characteristic U-shape of differential capacitance vs potential plots is apparent from Figure 5. Capacitance data were independent of the frequency in the range 2.5–100 Hz, the scatter being less than 5%. Since the potential of zero surface charge E_{pzc} (or the corresponding potential difference $\Delta_o^w\varphi_{pzc}$) is known from the surface tension measurements,[9] the surface charge density q can be evaluated by integrating the capacitance plot. Table II gives the results of this integration for the system consisting of 0.05 M LiCl in water and 0.05 M Bu_4NPh_4B in nitrobenzene, in which case $E_{pzc} = 0.270$ V (vs Bu_4N^+).[9] Surface charge data represent the basis for an analysis of double-layer effects in ion-transfer kinetics as discussed later.

TABLE II: Surface Charge Density and Components of Interfacial Potential Difference Based on Gouy–Chapman or Modified Poisson–Boltzmann Theories (in Parentheses)[a]

E,[b] mV	$\Delta_o^w\varphi$, mV	q^w, mC m^{-2}	φ_2^w, mV	φ_2^o, mV	φ_1, mV
160	−110	−22.0	39 (38)	−54 (−44)	−18 (−28)
180	−90	−16.8	31 (29)	−44 (−35)	−16 (−26)
200	−70	−12.4	23 (23)	−34 (−28)	−13 (−19)
220	−50	−8.6	14 (16)	−24 (−20)	−11 (−14)
240	−30	−5.1	10 (11)	−15 (−12)	−6 (−7)
260	−10	−1.7	3 (4)	−5 (−4)	−2 (−2)
270	0	0	0 (0)	0 (0)	0 (0)
280	10	1.2	−2 (−4)	3 (3)	4 (4)
300	30	5.0	−10 (−10)	14 (12)	6 (8)
320	50	8.4	−16 (−17)	24 (20)	11 (14)
340	70	11.9	−22 (−22)	32 (26)	15 (22)
360	90	15.6	−29 (−28)	41 (33)	21 (28)
380	110	19.6	−35 (−35)	49 (40)	26 (35)
400	130	23.9	−42 (−41)	57 (47)	32 (42)
420	150	28.5	−48 (−48)	64 (53)	38 (50)
440	170	33.5	−54 (−54)	71 (59)	45 (58)
460	190	38.9	−60 (−58)	78 (65)	52 (66)
480	210	44.8	−66 (−65)	85 (71)	59 (75)

[a] Base electrolytes; 0.05 M LiCl in water, 0.05 M Bu_4NPh_4B in nitrobenzene. [b] Referred to Bu_4N^+ ion.

Results of surface tension[9] and impedance[18] measurements suggest that the modified Verwey–Niessen (MVN) model[19] offers a plausible picture of the interface between two immiscible electrolyte solutions (ITIES). According to this model a layer of solvent molecules (the inner layer) separates two ionic space charge regions (the diffuse double layer). The interfacial potential difference splits into three contributions

$$\Delta_o^w\varphi = \varphi_1 + \varphi_2^o - \varphi_2^w \qquad (10)$$

where $\varphi_1 = \varphi(x_2^w) - \varphi(x_2^o)$ is the potential difference across the inner layer, i.e., between the hypothetical planes x_2^w and x_2^o separating the inner layer from the space charge regions, and $\varphi_2^w = \varphi(x_2^w) - \varphi(\text{w,bulk})$ and $\varphi_2^o = \varphi(x_2^o) - \varphi(\text{o,bulk})$ are the potential differences across the space charge regions in the aqueous or the organic solvent phase. The ion distribution function and the components of the interfacial potential difference were calculated by means of the Gouy–Chapman (GC)[20,21] and modified Poisson–Boltzmann (MPB)[22] theories. In the former case the calculations are relatively straightforward.[18] In the latter case we applied the MPB 4 version and the numerical procedure[22] for a primitive model electrolyte, which consisted of a continuum dielectric medium containing spherical ions of radii $r_{ion}^w = 0.2125$ nm or $r_{ion}^o = 0.425$ nm. The two space charge regions were considered as not overlapping, but the image forces were included. Results of these calculations are summarized in Table II. As expected,[23] the GC theory somewhat overestimates the potential difference across the space charge region. However, at the charge densities encountered here, the discrepancies between these two theories are rather small and in the case of water practically negligible. It is evident that the interfacial potential difference is spread mainly in the diffuse double layer.

Formal kinetics of the simple ion transfer is based on the first-order rate law

$$I/zFS = \vec{k}c^w - \overleftarrow{k}c^o \qquad (11)$$

where I is the electrical current, S is the interfacial area, and $\vec{k}$ or $\overleftarrow{k}$ are the apparent rate constants of the ion transfer from the

(18) Samec, Z.; Mareček, V.; Homolka, D. *J. Electroanal. Chem. Interfacial Electrochem.* **1985**, *187*, 31.
(19) (a) Gavach, C.; Seta, P.; d'Epenoux, B. *J. Electroanal. Interfacial Electrochem.* **1977**, *83*, 225. (b) Reid, J. D.; Melroy, O. R.; Buck, R. P. *J. Electroanal. Chem. Interfacial Electrochem.* **1983**, *147*, 71.
(20) Gouy, G. *C. R. Acad. Sci.* **1910**, *149*, 654.
(21) Chapman, D. L. *Philos. Mag.* **1913**, *25*, 475.
(22) Outhwaite, C. W.; Bhuiyan, L. B.; Levine, S. *J. Chem. Soc., Faraday Trans. 2* **1980**, *76*, 1388.
(23) Carnie, S. L.; Torrie, G. M. *Adv. Chem. Phys.* **1984**, *56*, 141.

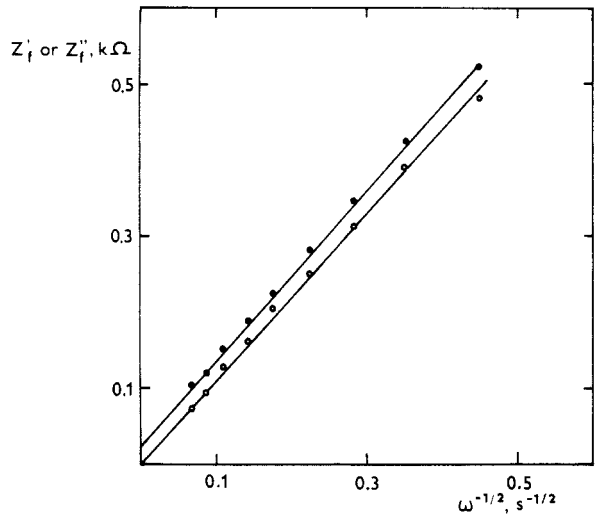

Figure 6. Plot of the real (●) and the imaginary (○) components of the faradaic impedance vs $\omega^{-1/2}$ for the transfer of Me_3EtP^+ across the interface between 0.05 M LiCl water and 0.05 M Bu_4NPh_4B in nitrobenzene.

aqueous to the organic solvent phase or the reverse. The rate constants are related to each other through[24]

$$\vec{k} = \tilde{k} \exp(-\Delta\vec{G}/RT) = \tilde{k} \exp[zF(E - E^\circ)/RT] \quad (12)$$

where $\Delta\vec{G}$ is the apparent reaction Gibbs energy. Equation 12 ensures that the Nernst potential (eq 7) will establish under equilibrium conditions ($I = 0$). Since the transport of the ion X^z in the solution is obviously controlled by the linear and semiinfinite diffusion, the corresponding faradaic impedance $\tilde{Z}_{fl}$ can be written as the sum of the charge-transfer resistance R_{ct} and the Warburg impedance $\tilde{Z}_W$[25]

$$\tilde{Z}_{fl} = R_{ct} + \tilde{Z}_W = R_{ct} + (1 - j)\rho\omega^{-1/2} \quad (13)$$

where

$$R_{ct} = \frac{RT}{z^2F^2S\vec{k}c^{o,w}} \quad (14)$$

and the transport parameter is defined as

$$\rho = \frac{RT}{2^{1/2}z^2F^2S}\left[\frac{1}{D^{o\,1/2}c^{o,o}} + \frac{1}{D^{w\,1/2}c^{o,w}}\right] \quad (15)$$

As follows from eq 13, plots of the real Z'_{fl} and the imaginary Z''_{fl} parts of the faradaic impedance $\tilde{Z}_{fl}$ vs $\omega^{-1/2}$ should give straight lines with an equal slope of ρ and with intercepts of $Z'_{fl} = R_{ct}$ and $Z''_{fl} = 0$, respectively. This was actually the case for all the ion-transfer systems measured. Typical plots are shown in Figure 6. Extrapolated values of Z'_{fl} at $\omega^{-1/2} = 0$ were then used to evaluate the rate constant $\vec{k}$ through eq 14. Since plots of log $\vec{k}$ vs the equilibrium potential E gave straight lines (Figure 7), two kinetic parameters were chosen to characterize the formal kinetics of the simple ion transfer, namely the apparent rate constant $k^0_{app} = \vec{k}(E^\circ) = \vec{k}(E^\circ)$ at the standard potential $E = E^\circ$, and the apparent charge-transfer coefficient

$$\alpha_{app} = (RT/zF)(\partial \ln \vec{k}/\partial E) \quad (16)$$

Their values are summarized in Table I.

Discussion

Thermodynamics and Transport. The standard potential difference $\Delta^w_o\varphi^\circ$ of the simple ion transfer is related to the standard

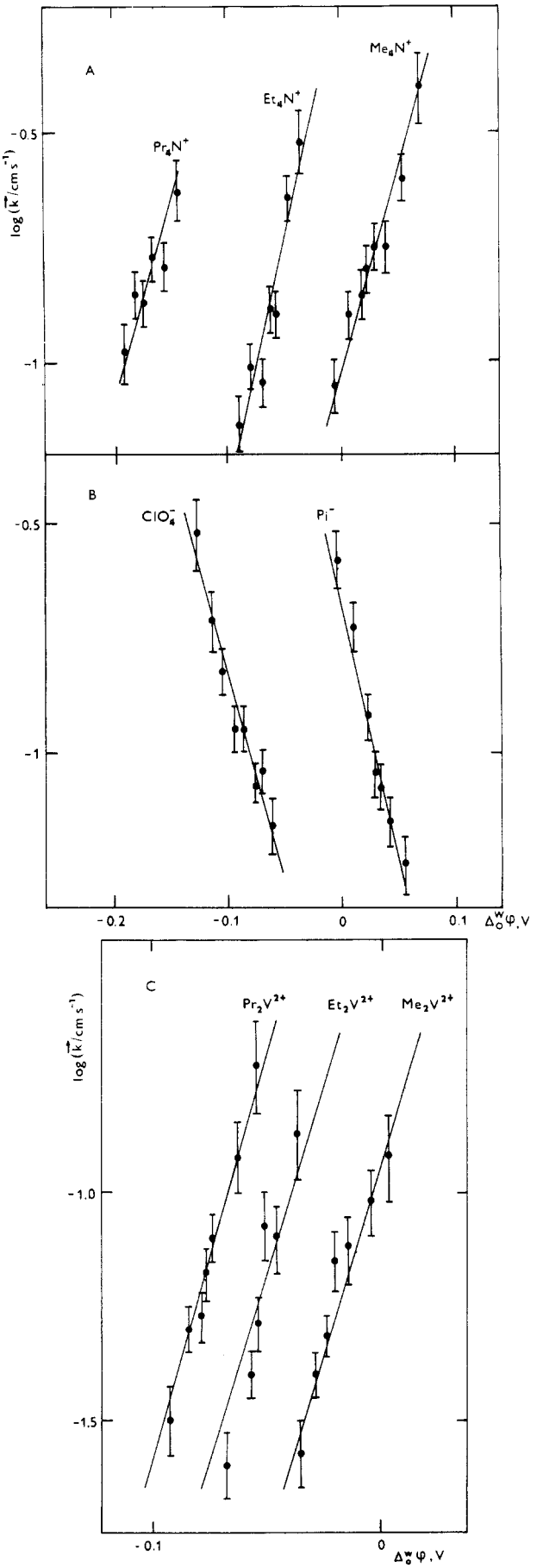

Figure 7. Apparent rate constant $\vec{k}$ vs the potential difference $\Delta^w_o\varphi$ for the transfer of (A) monovalent cations, (B) monovalent anions, and (C) divalent cations from the solution of 0.05 M LiCl in water to the solution of 0.05 M Bu_4NPh_4B or Ph_4AsDCC in nitrobenzene.

(24) Samec, Z. *J. Electroanal. Chem. Interfacial Electrochem.* **1979**, *99*, 197.

(25) Sluyters-Rehbach, M.; Sluyters, J. H. In *Comprehensive Treatise of Electrochemistry*; Yeager, E.; Sarangapani, S.; Eds.; Plenum Press: New York, 1984; pp 177–292.

Gibbs energy of ion transfer from water to organic solvent $\Delta\vec{G}^\circ_{tr}$ by

$$\Delta^w_o\varphi^\circ = \Delta\vec{G}^\circ_{tr}/zF \quad (17)$$

Evaluation of either of these quantities from partition, solubility, or electrochemical measurements is inevitably based on an extrathermodynamic hypothesis. The assumption that Ph_4As^+ and Ph_4B^- have equal Gibbs energies of transfer between any pair of solvents[26] (−35.9 kJ mol^{-1} in water–nitrobenzene system[27]) has been widely used[28] and underlies the present discussion too. In addition to the Ph_4As^+ ion, the Bu_4N^+ ion has often been used as the reference ion in electrochemical studies, for which the standard potential difference $\Delta^w_o\varphi^\circ = -0.248$ V was calculated[15,29] from partition data.[27] The latter value has been corrected[14] by taking $\Delta^w_o\varphi^\circ = -0.275$ V, on the basis of which much better agreement was reached between electrochemical data and those derived from partition measurements. An independent experimental test of "Ph_4AsPh_4B" hypothesis is provided by measurements of the zero-charge potential E_{pzc}.[30] The point here is that the potential difference $\Delta^w_o\varphi$ across the water–nitrobenzene interface is spread mainly in the diffuse double layer;[9,14,18,19] i.e., when the surface charge density is zero (electrocapillary maximum), the potential difference $\Delta^w_o\varphi$ should be close to zero too. In fact, by using the hypothesis above, the value of $\Delta^w_o\varphi_{pzc} \approx 0$ was derived from surface tension[9,19] or impedance[14,18] measurements in the presence of various electrolytes in water and nitrobenzene.

From the present voltammetric or potentiometric measurements the following values of $\Delta\vec{G}^\circ_{tr}$ (in kJ mol^{-1}) were obtained for Me_4N^+, Et_4N^+, Pr_4N^+, Pi^- (picrate), and ClO_4^-, which agree well with partition data[27] (in parentheses): 2.9 (3.4), −6.4 (−5.7), −15.6 (−15.7),[35] −4.1 (−4.6), and 7.9 (8.0), respectively. Standard Gibbs energies of transfer 0.9, −1.9, −4.8, and −8.1 kJ mol^{-1} were found analogously for Me_4P^+, Me_3EtP^+, Me_3PrP^+, and Me_3BuP^+ ions, for which no partition data are available. By taking into account the ion association, the values of $\Delta\vec{G}^\circ_{tr} = 2F\Delta^w_o\varphi^\circ$ for Me_2V^{2+}, Et_2V^{2+}, and Pr_2V^{2+} were −2.9, −8.3, and −11.2 kJ mol^{-1}, respectively.

Obviously, the standard Gibbs energy of transfer reflects an ascending hydrophobic character of ions as the number of CH_2 groups in the aliphatic carbon chains increases. Its structure-additive property is illustrated by almost identical average decrements of −2.4, −3.1, or −2.1 kJ per CH_2 group in R_4N^+, Me_3RP^+, or R_2V^{2+} homologous series. These results agree well with the values of −2.5[32] or −2.6[33] kJ per CH_2 group reported previously for the $R_1R_2R_3R_4N^+$ series.

Diffusion coefficients of ions in water, and analogously those in nitrobenzene, show no striking difference and seem to reflect primarily the size of ions and the viscosity of the medium. Such a behavior is predicted by an Einstein–Stokes type of equation,[34,35] namely for a spherical ion of radius r_{ion}

$$D = kT/c\pi\eta r_{ion} \quad (18)$$

where kT is the Boltzmann factor and η is the viscosity coefficient (1.005 or 2.03 cP at 293 K for water or nitrobenzene, respectively). Provided that both ion and solvent are spherical, c is predicted to depend on the ratio of radii r_s/r_{ion} of solvent and ion according to the simple relationship[35]

$$c = 6/[(3r_s/2r_{ion}) + 1/(1 + r_s/r_{ion})] \quad (19)$$

Obviously, when the size of the solvent is much smaller than that of the ion, so that the solvent can be considered as the hydrodynamic continuum, the numerical factor $c = 6$. The ion radius r_{ion} was calculated by eq 18 and 19 from diffusion coefficient in water (Table I) for the radius of water molecule $r_w = 0.155$ nm. The former was found to correlate with the ion radius $\bar{r}_{ion}$ derived from molar volumes. In particular, the ratio $\bar{r}_{ion}/r_{ion}$ is close to unity and equals to (in parentheses ion radii from molar volumes[36] in nm): 0.81 (0.258), 0.95 (0.310), 1.01 (0.352), or 1.08 (0.245) for Me_4N^+, Et_4N^+, Pr_4N^+, or ClO_4^-, respectively. Moreover, except for Pr_2V^{2+} the ratio of diffusion coefficients D^w/D^o for all other ions falls in the range 2.0–2.6, i.e., not far from the ratio of viscosity coefficients for pure solvents, $\eta^o/\eta^w = 2.03$.

Apparent Ion-Transfer Rates. On the basis of present results we conclude that the ion transfer across the ITIES is rather fast. Somewhat lower values of the apparent rate constant k^0_{app} (in cm s^{-1}) for Me_4N^+ (6.5×10^{-2}),[7a] Et_4N^+ (3.7×10^{-2}),[5b] Pr_4N^+ (2.6×10^{-2}),[5b] and Pi^- (3.7×10^{-2})[7b] have been derived from potential sweep measurements. Here, the uncompensated ohmic potential drop is probably the main source of the experimental error. Moreover, the change in the position and the shape of the interface due to the potential dependence of the surface tension[9] can give rise to an additional ohmic potential drop, or to the convective contribution to the ion transport.[10] Apparent rate constants for the Me_4N^+ (5.6×10^{-4}),[46] Et_4N^+ (2.3×10^{-3}),[6a] and Pr_4N^+ (2.1×10^{-3})[6a] ion transfer have been obtained without properly taking into account the existence of the solution resistance and are quite incorrect. Surprisingly, the preliminary results of equilibrium impedance measurements[8] also indicate rather slow ion transfer with the apparent rate constant about 5×10^{-3} cm s^{-1}. However, the use of platinum wires as reference electrodes[8,37] can be the source of error, because the easy polarization of the platinum electrodes can lead to a pseudokinetic behavior.

Effect of Electrical Double-Layer Structure. The diffusion double layer is rapidly established[38] and kinetic effects connected with its relaxation are far beyond the detection limit (>1 ms) of present impedance measurements. Consequently, a slow step which would account for the kinetic behavior observed here must be located in the inner-layer region. The three-step (or four-position) mechanism of the simple ion transfer across the ITIES appears to be a good approximation

$$X^z(w,b) \overset{\text{fast}}{\rightleftharpoons} X^z(w,x_2^w) \overset{\text{rds}}{\rightleftharpoons} X^z(o,x_2^o) \overset{\text{fast}}{\rightleftharpoons} X^z(o,b) \quad (20)$$

where b denotes the bulk of the solution. The rate-determining step (rds) in this sequence is the ion jump over the inner layer ($x_2^w \rightarrow x_2^o$). The four-position mechanism of solute transfer across the liquid–liquid interface was proposed by Buck.[39] The existence of the space charge distribution in the double layer was considered and the Frumkin-type correction of the apparent rate constant was introduced later.[24,40] This correction can be written as[24]

$$\vec{k} = \vec{k}_t g(x_2^w) \quad (21)$$

where $\vec{k}_t$ is the rate constant for the rate-determining step and $g(x_2^w)$ is the ion distribution function at the outer Helmholtz plane on the aqueous side of the interface. By use of the GC theory for the MVN model, $g(x_2^w)$ can be expressed[19a]

$$\varphi_2^w = -(RT/zF)\ln g(x_2^w)$$

$$= (RT/zF)\ln\frac{1 + p\exp[-F(\Delta^w_o\varphi - \varphi_1)/2RT]}{1 + p\exp[F(\Delta^w_o\varphi - \varphi_1)/2RT]} \quad (22)$$

where $p = (\epsilon^o c^{0,o}/\epsilon^w c^{0,w})^{1/2}$, ϵ's are dielectric constants, and c^0's are base electrolyte concentrations. When the potential depen-

(26) Parker, A. J. *Chem. Rev.* **1969**, *69*, 1.
(27) Rais, J. *Collect. Czech. Chem. Commun.* **1971**, *36*, 3253.
(28) Marcus, Y. *Pure Appl. Chem.* **1983**, *55*, 977.
(29) Hung, Le. Q. *J. Electroanal. Chem. Interfacial Electrochem.* **1980**, *115*, 159.
(30) Girault, H. H. J.; Schiffrin, D. J. *Electrochim. Acta* **1986**, *31*, 1341.
(31) Abraham, M. A. *J. Chem. Soc., Perkin Trans. 2* **1972**, 1343.
(32) Osakai, T.; Kakutani, T.; Nishiwaki, Z.; Senda, M. *Bunseki Kagaku* **1983**, *32*, E81.
(33) Iwamoto, E.; Ito, K.; Yamamoto, Y. *Z. Phys. Chem.* **1981**, *85*, 894.
(34) Robinson, R. A.; Stokes, R. H. *Electrolyte Solutions*, 2nd ed.; Butterworths: London, 1959; pp 43 and 125.
(35) (a) Gierer, A.; Wirtz, K. *Z. Naturforsch. A* **1953**, *8*, 522. (b) Spernol, A.; Wirtz, K. *Z. Naturforsch. A* **1953**, *8*, 532.
(36) Abraham, M. H.; Liszi, J. *J. Inorg. Nucl. Chem.* **1981**, *43*, 143.
(37) Melroy, O. R.; Bronner, W. E.; Buck, R. P. *J. Electrochem. Soc.* **1983**, *130*, 373.
(38) Macdonald, J. R. *Trans. Faraday Soc.* **1970**, *66*, 943.
(39) Buck, R. P. *Crit. Rev. Anal. Chem.* **1975**, *5*, 323.
(40) d'Epenoux, B.; Seta, P.; Amblard, G.; Gavach, C. *J. Electroanal. Chem. Interfacial Electrochem.* **1979**, *99*, 77.

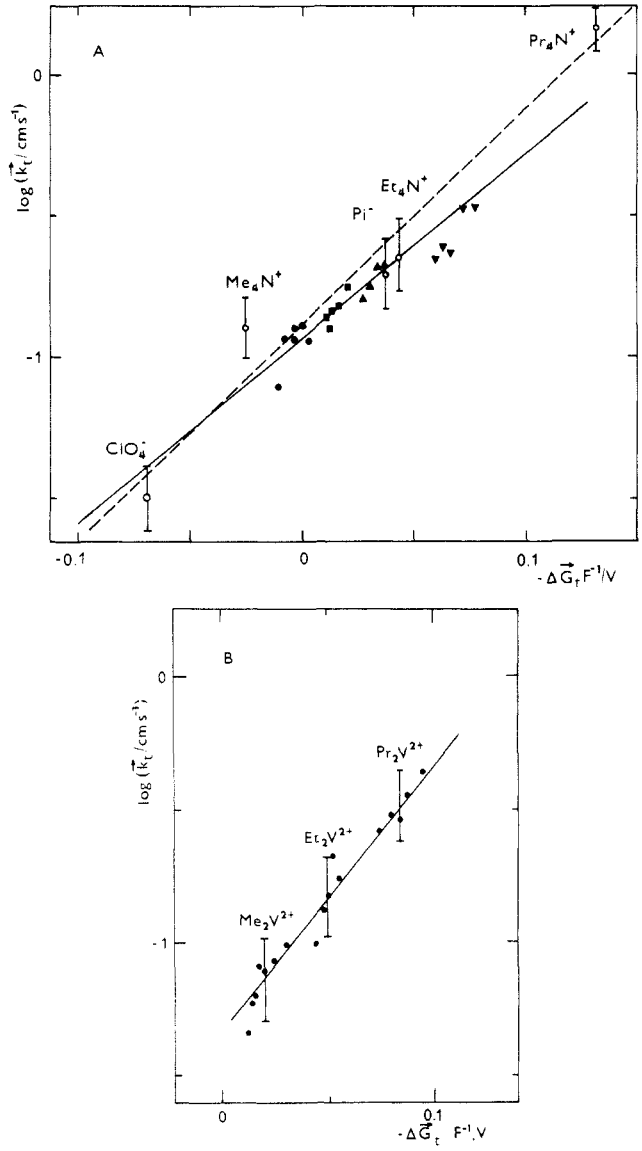

Figure 8. Correlation of the rate constant $\vec{k}_t$ with the Gibbs energy of ion transfer across the inner layer $\Delta\vec{G}_t = -zF(\varphi_i - \Delta_o^w\varphi^\circ)$ for (A) monovalent and (B) divalent ions. Dashed line: linear regression for Me_4N^+, Et_4N^+, Pr_4N^+, ClO_4^-, and Pi^- ions. Full lines: linear regressions for Me_4P^+ (●), Me_3EtP^+ (■), Me_3PrP^+ (▲), and Me_3BuP^+ (▼); or Me_2V^{2+}, Et_2V^{2+}, and Pr_2V^{2+} ions.

dence of $\vec{k}_t$ is specified, eq 21 and 22 can be used to illustrate the effect of the double layer on the apparent rate constant.[8,41,42] In particular, when the electrical part of the ion Gibbs energy change across the inner layer $\Delta\vec{G}_t$ is negligible

$$\Delta\vec{G}_t = \Delta\vec{G}^\circ_{tr} - zF\varphi_i = -zF(\varphi_i - \Delta_o^w\varphi^\circ) \qquad (23)$$

one can expect that the rate constant $\vec{k}_t$ depends little on the potential E, and the apparent charge-transfer coefficient (eq 14) $\alpha_{app} \approx 0.5$.[8,41] Such a value has been actually found for all the ions studied (Figure 7, Table I).

Properties of the Kinetic Barrier. It has been impossible to make any conclusion about the molecular mechanism of the ion transfer across the inner layer from the study of a single ion-transfer reaction. We have suggested[5c] that the correlation of $\vec{k}_t$ with $\Delta\vec{G}_t$ for a homologous series of ions could provide some insight into this mechanism. The point is that the slope of such correlation can be related to the symmetry or the position of the kinetic barrier in the rate-determining step. We shall show that this correlation applies to ions of various structures and charge numbers.

Figure 8 presents plots of log $\vec{k}_t$ vs $\Delta\vec{G}_t$ for all ions studied. The MPB values for φ_2^w and φ_i in eq 21 to 23 were taken from Table II. Kinetic data for the Pi^- ion transfer were taken from ref 10. When a particular ion-trasfer reaction is inspected, it is clear that changes in $\Delta\vec{G}_t$ and $\vec{k}_t$ are rather small to provide a meaningful correlation. This is because the inner-layer potential difference φ_i or the Gibbs energy change $\Delta\vec{G}_t$ (eq 23) is not very sensitive to variations in the potential E. On the other hand, the kinetic data for various ions, which differ considerably in $\Delta\vec{G}_t$ due to different Gibbs energies of ion transfer, fall on a single straight line with the slope corresponding to the true charge-transfer coefficient $\alpha_t = -RT(\partial \ln \vec{k}_t/\partial\Delta\vec{G}_t) = 0.47$, 0.40, or 0.58 for tetraalkylammonium, trimethylalkylphosphonium, and dialkyldipyridinium ions, respectively. To some degree of uncertainty, rate constants for individual ion-transfer reactions display analogous trends, e.g., for the picrate ion transfer the value of $\alpha_t = 0.6 \pm 0.1$ was reported.[10] The structure and the charge number of the ion seem to influence the ion-transfer rate mainly indirectly through $\Delta\vec{G}_t$.

Various kinetic models of the rate-determining step have been proposed.[6b,24,42-45] Melroy and Buck[6b] used the transition-state theory to express the rate constant $\vec{k}_t$ by

$$\vec{k}_t = k_0 \exp(-\Delta\vec{G}^*_t/kT) = \kappa(kT/h)\exp(-\Delta\vec{G}^*_t/kT) \qquad (24)$$

The standard Gibbs energy of activation $\Delta\vec{G}^*_t$ was divided into the chemical ($\Delta\vec{G}^*_c$) and electrical contributions and the latter was represented as some fraction of the electrical energy change across the inner layer: $\Delta\vec{G}^*_t = \Delta\vec{G}^*_t + \alpha_c zF\varphi_i$. Apart from the unclear physical meaning of the preexponential factor $\kappa(kT/h)$, eq 24 does not predict the Brønsted-like correlation shown in Figure 8, which is obviously implicit in the term $\Delta\vec{G}^*_c$. With reference to the transition-state theory of diffusion,[46] Girault and Schiffrin[42] used a similar expression for $\vec{k}_t$, but with $k_0 = (kT/h)d$, where d is the distance between two equilibrium positions of the ion. These authors have also introduced the "chemical" charge-transfer coefficient α_c, $\Delta\vec{G}^*_t = \alpha_c\Delta\vec{G}^\circ_{tr}$, which actually might control the slope of the plot in Figure 8. However, it should be noted that the question of validity of the rate equation, eq 24, remains unsolved within the framework of the transition-state theory. In fact, this type of expression can be derived for a molecular kinetic model based either on the tunnel hopping of the ion from one cage formed by solvent molecules to the neighbor cage[47] or on the nonadiabatic subbarrier penetration of an ion through the inner layer region.[24] A more involved quantum-mechanical treatment[45] shows that all these models could describe transfer processes of light ions (H^+, Li^+) or the processes occurring in well-structured media, e.g., in solid ionic conductors. In liquids no well-defined initial and final states of an ion can be specified, and the meaning of the transition state and the Gibbs energy of activation for the transfer process becomes obscure.

Hence, it seems more appropriate to treat the ion transport as the brownian motion by the stochastic method.[48] Provided that the characteristic frequency of ionic motion ω is low, so that $\omega \ll \xi/m$, where $\xi = kT/D$ is the friction coefficient of medium and m is the ionic mass, the equilibrium distribution of ionic velocities is established. Then the probability $p = p(x,t)$ that the ion has the coordinate x at a time t is governed by Smoluchowski equation[48]

$$\partial p/\partial t = \partial J/\partial x \qquad (25)$$

where the ionic flux J

$$J = (kT/\xi)[\partial p/\partial x + (p/kT)(\partial V/\partial x)] \qquad (26)$$

(41) Koryta, J. *Anal. Chim. Acta* **1982**, *139*, 1.
(42) Girault, H. H. J.; Schiffrin, D. J. *J. Electroanal. Chem. Interfacial Electrochem.* **1985**, *195*, 213.
(43) Gurevich, Yu. Ya.; Kharkats, Yu, I. *J. Electroanal. Chem. Interfacial Electrochem.* **1986**, *200*, 3.
(44) Samec, Z.; Kharkats, Yu. I.; Gurevich, Yu. Ya. *J. Electroanal. Chem. Interfacial Electrochem.* **1986**, *204*, 257.
(45) Kuznetsov, A. M.; Kharkats, Yu. I. Reference 3, p 11.
(46) Stearn, A. E.; Eyring, H. *J. Phys. Chem.* **1940**, *44*, 955.
(47) Schmidt, P. P. *J. Chem. Soc. Faraday Trans. 2* **1984**, *80*, 157, 181.
(48) Gardiner, C. W. In *Handbook of Stochastic Methods for Physics, Chemistry and Natural Sciences*; Haken, H., Ed.; Springer-Verlag: Berlin, 1985; Vol. 13.

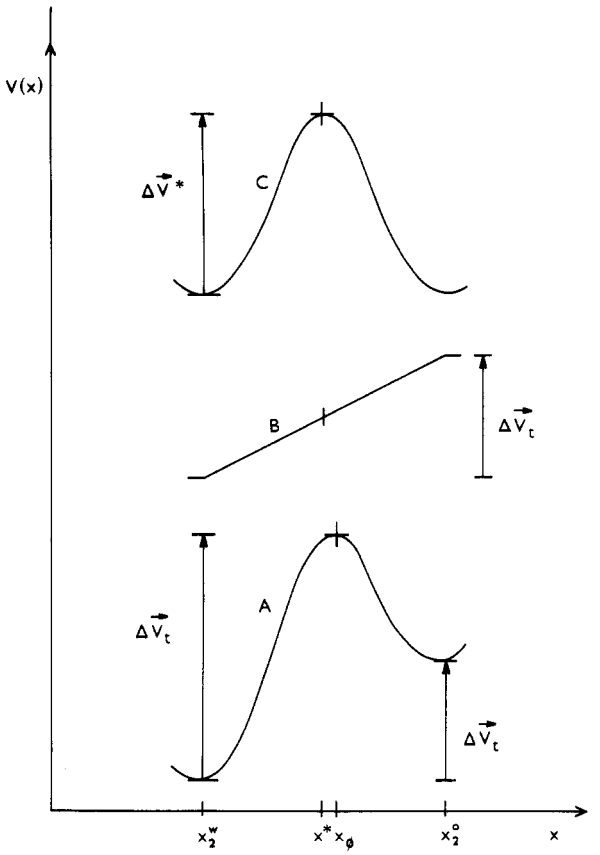

Figure 9. Schematic representation of the potential energy barrier to ion transfer across the inner layer (A) as the superposition of the linear potential connected with the long-range electrostatic interactions (B) and the barrier arising from the short-range repulsive interactions between the ion and solvent molecules in the inner layer (C).

and $V = V(x)$ is the potential energy of the ion. The analytical solution has been obtained assuming that the transfer process is stationary:[43,44] $\partial p/\partial t = 0$, J = constant. Actually, in that case the probability p takes the form of the Boltzmann equation: p_s = const × $\exp(-V/kT)$. The potential energy $V(x)$ of the ion in the inner layer was considered as a superposition of the potential energy barrier arising from the short-range repulsive interactions between ion and solvent molecules in the inner layer, and the linear potential connected with the long-range electrostatic interactions, inclusive of the contribution of the polar solvent around the ion (Figure 9).[44] The constant field treatment of the long-range interactions is somewhat an oversimplification, e.g., the resolvation may give rise to nonlinear effects. Near to its top, $V(x)$ was approximated by the quadratic function of the ion coordinate x. The equation for the rate constant is then formally identical with eq 24,[44] where

$$k_0 = (m\omega^*/\xi^*)Z = (m\omega^*/\xi^*)(kT/2\pi m)^{1/2} \quad (27)$$

$$\Delta\vec{G}^*_t = \Delta\vec{V}^* + (x^* - x_2^w)d^{-1}\Delta\vec{V}_t + \Delta\vec{V}_t^2/2m\omega^{*2}d^2 \quad (28)$$

Z is the collision frequency, $\omega^* = [(1/m)(\partial^2 V/\partial x^2)^*]^{1/2}$ is the frequency of the ion vibration at $x = x^*$, $d = x_2^o - x_2^w$ is the inner-layer thickness, $\Delta\vec{V}_t = V(x_2^o) - V(x_2^w)$ is the difference between the equilibrium potential energy prior to and after the jump, x^* is the ion coordinate corresponding to the potential energy maximum at $\Delta\vec{V}_t = 0$, and $\Delta\vec{V}^* = V(x^*) - V(x_2^w)$ is the activation energy at $\Delta\vec{V}_t = 0$. $\Delta\vec{V}_t$ is the sum of the resolvation energy and the electrostatic energy change ($zF\varphi_i$); i.e., it is practically identical with $\Delta\vec{G}_t$ (eq 23).

The frequency ω^* was estimated[12] from the relationship $(1/2)m\omega^{*2}\Delta x^2 \approx kT$, where Δx is of the order of magnitude of intermolecular distances in liquids, e.g., $\Delta x \approx 2r_w = 0.310$ nm. The friction coefficient was estimated as $\xi^* = kT/D^w$. For monovalent ions studied the frequency ω^* falls in the range (3.7–6.6) × 10^{11} s^{-1}, and dimensionless hydrodynamic factor $(m\omega^*/\xi^*)$ is much less than unity, i.e., $m\omega^*/\xi^* = (0.6–1.8) \times 10^{-2}$. The resulting values of the preexponential factor k_0 are listed in Table III. It should be noted that the transition-type treatments[6b,42] predict much higher values, e.g., $(kT/h)\Delta x \approx 1.8 \times 10^5$ cm s^{-1}.

TABLE III: Parameters of Stochastic Theory for Monovalent Ion Transfer across the Water/Nitrobenzene Interface

ion	$\Delta\vec{G}_tF^{-1}$, mV	$\vec{k}_t$, cm s^{-1}	k_0, cm s^{-1}	$\Delta\vec{V}^*$, kJ mol^{-1}
Me_4N^+	−25	0.120	70	14.3
Et_4N^+	−44	0.240	68	15.8
Pr_4N^+	−130	1.38	63	15.5
Pi^-	−38	0.182	44	15.2
ClO_4^-	68	0.030	112	16.8

The inner-layer thickness was estimated as $d = (r^w_{ion} + r^o_{ion}) + 2r_w + 2r_{org} \approx 1.34$ nm, where $2r_{org} = 0.555$ nm is the diameter of nitrobenzene molecule calculated from its molar volume and $r^w_{ion} \approx r^o_{ion} \approx 0.2$ nm. An estimate shows that the ratio of the quadratic and the linear terms in eq 28 is rather small. Since the preexponential factor does not vary much, the true charge-transfer coefficient becomes $\alpha_t = -RT(\partial \ln \vec{k}_t/\partial\Delta\vec{V}_t) \approx (x^* - x_2^w)d^{-1}$. The value of $\alpha_t \approx 0.5$ calculated from the slope of plots displayed in Figure 8 indicates that this configuration is located just amidst the positions $x = x_2^w$ and $x = x_2^o$ of the outer Helmholtz planes. Upon substituting 0.5 for $(x^* - x_2^o)d^{-1}$ in eq 28 and neglecting the quadratic term, the values of the activation energy $\Delta\vec{V}^*$ of 14–17 kJ mol^{-1} were calculated from kinetic data by using eq 24 (Table III). The origin of the kinetic barrier is most probably connected with the existence of the compact solvent layer at the interface. An extension of this analysis to the transfer of R_2V^{2+} cations is not straightforward because of the bimolecular mechanism of the charge transfer (eq 8).

Salt Extraction Kinetics. An obvious application of results presented in the foregoing sections concerns the liquid/liquid interfacial kinetics of salt extraction,[49] e.g., that described by

$$B^+(w) + A^-(w) \rightleftarrows B^+(o) + A^-(o) \quad (29)$$

During the extraction process no electrical current flows through the system, i.e.

$$I_+ + I_- = 0 \quad (30)$$

where I_+ is the current corresponding to the cation and I_- to the anion of a salt BA. In the course of this process the ratio of salt concentrations $c^o/c^w = c^o_+/c^w_+ = c^o_-/c^w_-$, and hence both the interfacial potential difference $\Delta^w_o\varphi$ (cf. eq 7) and the ion-transfer rate I_i (eq 11) vary till the equilibrium values of the distribution coefficient $K^{o,w}$ or the distribution potential $\Delta^w_o\varphi_{distr}$ are reached.[49] For a 1:1 BA salt[50]

$$K^{o,w} = (c^{0,o}/c^{0,w})(\gamma^o_\pm/\gamma^w_\pm) = \exp[-(\Delta\vec{G}^\circ_{tr,+} + \Delta\vec{G}^\circ_{tr,-})/2RT] \quad (31)$$

and

$$\Delta^w_o\varphi_{distr} = (\Delta^w_o\varphi^0_+ + \Delta^w_o\varphi^o_-)/2 + (RT/2F)\ln(\gamma^w_+\gamma^o_-/\gamma^o_+\gamma^w_-) \quad (32)$$

where $c^{0,s}$ denotes the equilibrium bulk concentration of the salt, γ^s_i of $\gamma^s_\pm$ is the activity coefficient or the mean activity coefficient in the phase s. As shown in the previous section, the charge-transfer coefficient $\alpha_t \approx$ const ≈ 0.5. The limiting rate of extraction of a 1:1 BA salt from water to the organic solvent ($c^o/c^w = 0$) is then given by (cf. also ref 49)

$$I_\pm/FS = \pm k^0 \exp(\mp F\varphi^w_2/RT) \exp[\pm\alpha_t F(\varphi_i - \Delta^w_o\varphi)/RT]c^w = k^{o,w}c^w \quad (33)$$

where $k^{o,w}$ is the extraction rate constant

$$k^{o,w} = (k^0_+k^0_-)^{1/2}(K^{o,w})^{\alpha_t} \quad (34)$$

(49) Koryta, J.; Skalický, M. *J. Electroanal. Chem. Interfacial Electrochem.* **1987**, *229*, 265.
(50) Karpfen, F. M.; Randles, J. E. B. *Trans. Faraday Soc.* **1953**, *49*, 823.

TABLE IV: Thermodynamic and Kinetic Parameters of Extraction of Simple Salts from Water to Nitrobenzene

salt	$K^{o,w}$	$\Delta_o^w\varphi$ distr, mV	$k^{o,w}$, cm s^{-1}
Me_4NClO_4	0.113	-28	0.050
Et_4NClO_4	0.728	-75	0.092
Pr_4NClO_4	5.07	-124	0.253
Me_4NPi	1.27	33	0.147
Et_4NPi	8.16	-14	0.269
Pr_4NPi	56.8	-63	0.737

and $k^0_i = k_0 \exp(-\Delta\vec{V}^*_i/kT)$. Table IV lists values of distribution coefficients, distribution potentials, and extraction rate constants for a series of perchlorates and picrates, which were calculated from thermodynamic and kinetic parameters of individual ion-transfer reactions obtained in this work. Since the constant k^0_i is approximately the same for all ions, the leading factor in the extraction rate is the distribution coefficient $K^{o,w}$. Our estimates differ considerably from those previously reported.[49] It should be noted that the authors[49] used a somewhat different set of values of ionic rate constants and an incorrect value of the standard potential difference for the picrate ion transfer.

It is evident that the extraction of the simple salt from water to a high-permittivity solvent is a rather fast process, the kinetics of which is experimentally accessible only when a rapidly stirred system is used, enabling the separation of kinetic and transport contributions. No reliable experimental kinetic data on these processes have been reported.

Registry No. Me_4N^+, 51-92-3; Et_4N^+, 66-40-0; Pr_4N^+, 13010-31-6; Me_4P^+, 32589-80-3; Me_3EtP^+, 79826-63-4; Me_3PrP^+, 44519-38-2; Me_3BuP^+, 122624-00-4; ClO_4^-, 14797-73-0; Me_2V^{2+}, 4685-14-7; Et_2V^{2+}, 46713-38-6; Pr_2V^{2+}, 46903-41-7; LiCl, 7447-41-8; Bu_4NPh_4B, 15522-59-5; Ph_4AsDCC, 76598-08-8; H_2O, 7732-18-5; Pi^-, 14798-26-6; Me_4NClO_4, 2537-36-2; Et_4NClO_4, 2567-83-1; Pr_4NClO_4, 15780-02-6; Me_4NPi, 733-60-8; Et_4NPi, 741-03-7; Pr_4NPi, 747-43-3; nitrobenzene, 98-95-3.

Theoretical Nets with 18-Ring Channels: Enumeration, Geometrical Modeling, and Neutron Diffraction Study of $AlPO_4$-54

James W. Richardson, Jr.,*,†,‡ Joseph V. Smith,‡ and Joseph J. Pluth‡

Department of Geophysical Sciences, The University of Chicago, Chicago, Illinois 60637, and IPNS Division, Argonne National Laboratory, Argonne, Illinois 60439 *(Received: November 22, 1988; In Final Form: April 28, 1989)*

The framework topology of aluminophosphate no. 54 is the same as that of the aluminophosphate-based family of molecular sieves denoted VPI-5. It corresponds to that of theoretical net 81(1), now numbered 520, which has an 18-ring channel. Unit cell parameters for as-synthesized $AlPO_4$-54 are a = 19.009 (2) Å, c = 8.122 (1) Å, V = 2541.63 Å^3. $AlPO_4$-54 dehydrated at 275 °C has lattice parameters a = 18.549 (1) Å, c = 8.404 (1) Å, V = 2504.13 Å^3. The crystal structure of dehydrated $AlPO_4$-54 was determined from time-of-flight neutron diffraction data. The 13 theoretical nets with crankshaft chains that fit the hexagonal geometry and cell dimensions of $AlPO_4$-54 were considered as possible models for the structure. Only net 520 yielded a theoretical powder diffraction pattern that matched the data for $AlPO_4$-54. A Rietveld refinement for disordered Al,P in space group $P6_3/mcm$ converged, but the uncertainties in distances and angles are high. The $AlPO_4$-54 framework contains tetrahedrally coordinated Al and P at the vertices of a 3D net obtained by replacing each edge of a $(4.4.18)_1(4.6.18)_2$ 2D net by a crankshaft chain. The average free diameter across the 18-ring channel is 12.5 Å. (Al,P)-O bond distances from the Rietveld refinement range from 1.44 to 1.70 Å with a mean value of 1.60 Å, and (Al,P)-O-(Al,P) angles range from 132 to 180°. Refinement assuming strict alternation of Al and P space group $P6_3cm$ was unsuccessful because of strong pseudosymmetry. The diffraction patterns for the hydrated and dehydrated varieties of $AlPO_4$-54 and for the aluminophosphate-based VPI-5 family are generally similar, but detailed variations of position and intensity indicate that structural changes deserve thorough study. For the present neutron diffraction data, Fourier analysis of a diffuse scattering component suggests weak association of water with framework oxygens, and incomplete dehydration.

Introduction

Theoretical nets containing wide channels and windows are of considerable interest as the potential basis of molecular sieves for separation of large molecules, and for catalytic reactions involving heavy fractions of petroleum. Two infinite series of four-connected nets with unlimited ring size were invented by Smith and Dytrych,[1] and others have been described briefly, but not presented yet in detailed form (reviewed in ref 2). A new family of aluminophosphate-based molecular sieves containing pores defined by 18 tetrahedrally linked atoms was described by Davis et al.[3,4] After completion of the present study, Crowder et al.[5] published X-ray powder diffraction data for an uncalcined silicon-containing member that matches a theoretical pattern calculated for atomic positions based on the 81(1) net of Smith and Dytrych. Independently we examined the structure of $AlPO_4$-54. We present a systematic enumeration of 13 theoretical structures with an 18-ring channel that generally fit the cell dimensions of both the VPI-5 family and $AlPO_4$-54. Although the theoretical diffraction patterns are similar to each other, only the 81(1) net has space group symmetry that matches the systematic absences of the observed X-ray powder data of the VPI-5 family. We give a Rietveld refinement of pulsed-neutron diffraction data for a dehydrated powder of the new aluminophosphate $AlPO_4$-54 using a model based on the 81(1) topology. It was synthesized in accordance with the general procedures set forth in U.S. Patent 4310440 (ref 6) using a dialkylamine templating agent. The combined observations on the VPI-5 family and on $AlPO_4$-54 demonstrate that they have the 81(1) framework topology in common. However, the names VPI-5 and $AlPO_4$-54 are retained

† Argonne National Laboratory.
‡ The University of Chicago.

(1) Smith, J. V.; Dytrych, W. J. *Nature* **1984**, *309*, 607-608.
(2) Smith, J. V. *Chem. Rev.* **1988**, *88*, 149-182.
(3) Davis, M. E.; Saldarriaga, C.; Montes, C.; Garces, J.; Crowder, C. *Nature* **1988**, *331*, 698-699.
(4) Davis, M. E.; Saldarriaga, C.; Montes, C.; Garces, J.; Crowder, C. *Zeolites* **1988**, *8*, 362-366.
(5) Crowder, C. E.; Garces, J. M.; Davis, M. E. *Adv. X-ray Anal.*, in press.
(6) Wilson, S. T.; Lok, B. M.; Flanigen, E. M. U.S. Patent 4310440, January 1982.

0022-3654/89/2093-8212$01.50/0